Chapter 6

Considerations on the dynamics of maser stars in our Galaxy.

A preliminary report on an ongoing study by
H.J. Habing, M. Messineo, G. van de Ven, M. Sevenster and K.H. Kuijken

6.1 Introduction

In this thesis we present results from a survey of SiO maser stars undertaken for the explicit reason to investigate stellar kinematics and dynamics in the inner regions of the Milky Way. This survey is a continuation of the thesis project of M. Sevenster in which she looked at 1612 MHz (18cm) for OH/IR stars with the VLA in the northern hemisphere and with the ATCA in the southern hemisphere (Sevenster et al. 1997a,b, 2001). The results of Sevenster's survey have been presented and analysed in several papers (Debattista et al. 2002; Sevenster et al. 1999; Sevenster 1999a).

In discussing the velocities of the SiO maser stars we came across a question that until now has not been studied in depth: can the line-of-sight velocities ($v_{\rm los}$)[1] of SiO and OH maser stars in the forbidden quadrants of the longitude-velocity, $(l - v)$, diagram be explained by a rotating bar, and if so, can they be used to constrain the parameters of this bar? A full answer requires two consecutive steps: a) to find a potential and orbits in this potential that will fill the required areas of the $(l - v)$ diagram; 2) to find a physical explanation why stars fill these orbits. To answer this question we have started numerical calculations of the orbits in a gravitational potential and compared the predicted longitudes and line-of-sight velocities with those of the observations. Here we describe the first preliminary results of this ongoing study.

[1] We will use the term "line-of-sight velocity" instead of the more common term "radial velocity" to avoid confusion: in the kinematic and dynamical discussion "radial velocity" will be used for the motion along the radius vector from the Galactic Centre

6.2 Available evidence for a Galactic bar

To date, there is clear evidence that the Galactic gravitational field has a weak bar. This was first proposed by de Vaucouleurs (1964) based on the analysis of HI gas velocities and it was later confirmed by, e.g., Binney et al. (1991) and Bissantz et al. (2003). Other evidence comes from the asymmetry around $l = 0^\circ$ seen in the COBE data (e.g. Binney et al. 1997; Blitz & Spergel 1991; Weiland et al. 1994), star counts (Nakada et al. 1991; Whitelock & Catchpole 1992), and microlensing studies (Paczynski et al. 1994).

Stellar maser emission provides a unique tool for studying stellar kinematics. Unbiased samples of stellar line-of-sight velocities in the inner Galaxy are obtained through stellar OH and SiO maser searches, and these are not affected by interstellar extinction. In this small chapter we focus on the kinematics and spatial distribution of maser stars, whose properties have been discussed in the previous chapters or in the existing literature.

6.2.1 Asymmetry in the longitude distribution of maser stars

The data-set resulting from the OH/IR maser surveys by Sevenster et al. (1997a,b, 2001) uniformly covers the entire longitude range from -45° to $+45^\circ$. It can therefore be used very well to study a possible symmetry in star counts around $l = 0^\circ$. By plotting $l/|l|$ against $|l|$ in a cumulative fashion, a deviation from (axial) symmetry in the inner Galaxy shows up as a non–horizontal section. In part of the sample ($-10^\circ < l < 10^\circ$) an asymmetry was found that could be explained most naturally by a triaxial (m=2) component in the inner Galaxy, rather than a m=1 asymmetry (Sevenster 1999b). Here we present the same figure of the cumulative distribution (Fig. 6.1), but for a larger sample of OH/IR stars. The distribution is given for OH/IR stars as well as for MSX sources with AGB colours (as defined in Sevenster 2002) in the same region ($|b| < 3^\circ$). For OH/IR stars, there is an over-density at negative longitudes close to $l = 0^\circ$. At larger absolute longitudes, the over-density is at positive longitudes; the slope of the curve is positive. Around $l = 40^\circ$, the curve seems to level out, but this cannot be assessed in more detail as the sample doesn't go out far enough.

All these aspects are explained by a bar-like density distribution sampled out to distances well beyond the centre of the Galaxy, up to the far end of the bar. For the MSX sources, the initial negative slope is not seen and the curve starts to rise at lower longitudes. This may be explained by the same bar-like distribution sampled out to smaller distances (for a more detailed discussion see Sevenster 1999b).

Different models used to describe the density distribution of the bar lead to different values of the semi-major axis (a) of the bar and the viewing angle (ϕ), the angle between the line-of-sight and the major axis. However, they do not vary independently, and possible models seem to range very roughly from $\phi = 20^\circ$ and $a = 3$ kpc to $\phi = 50^\circ$ and $a = 2$ kpc; this relation is not necessarily linear. From measurements of the pattern speed (e.g. Debattista et al. 2002) we only have

an upper limit for the semi–major axis of about 3 kpc, so it will probably be hard to constrain the viewing angle as described here. However, if some parameters or even the functional form of the bar density are known from other arguments, this will limit the degrees of freedom considerably.

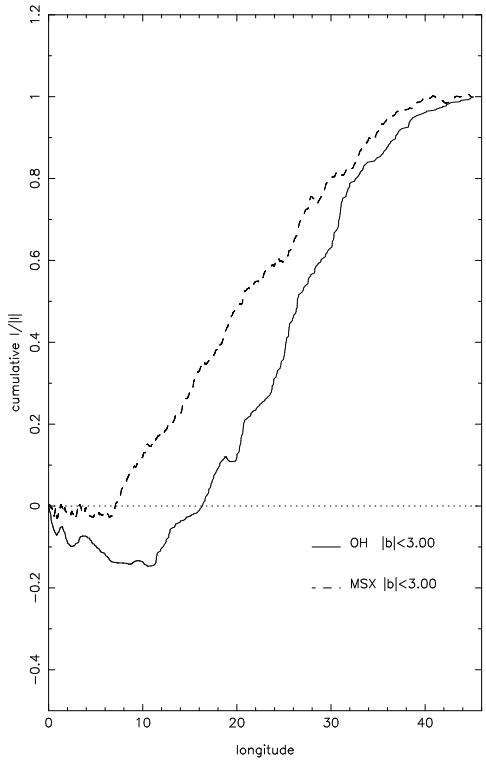

Figure 6.1: *On the horizontal axis the absolute longitude, $|l|$, is displayed and on the vertical axis the cumulative sum of $l/|l|$.*

6.2.2 Longitude–velocity diagram

We will use three observational $(l - v)$ diagrams. In the top panel of Fig. 6.2 the CO line spectrum from Dame et al. (2001) is shown; the middle panel shows the OH/IR stars observed by Sevenster and collaborators and the lower panel shows the SiO masers studied in this thesis.

If a cloud is located at the tangent point to the line of sight of a circular orbit around the Galactic centre (GC), its velocity vector will point entirely along the line-of-sight; the velocity at the tangent point is the highest velocity seen along a given line-of-sight. It will be called the terminal velocity, $v_{\rm term}$. An analytic

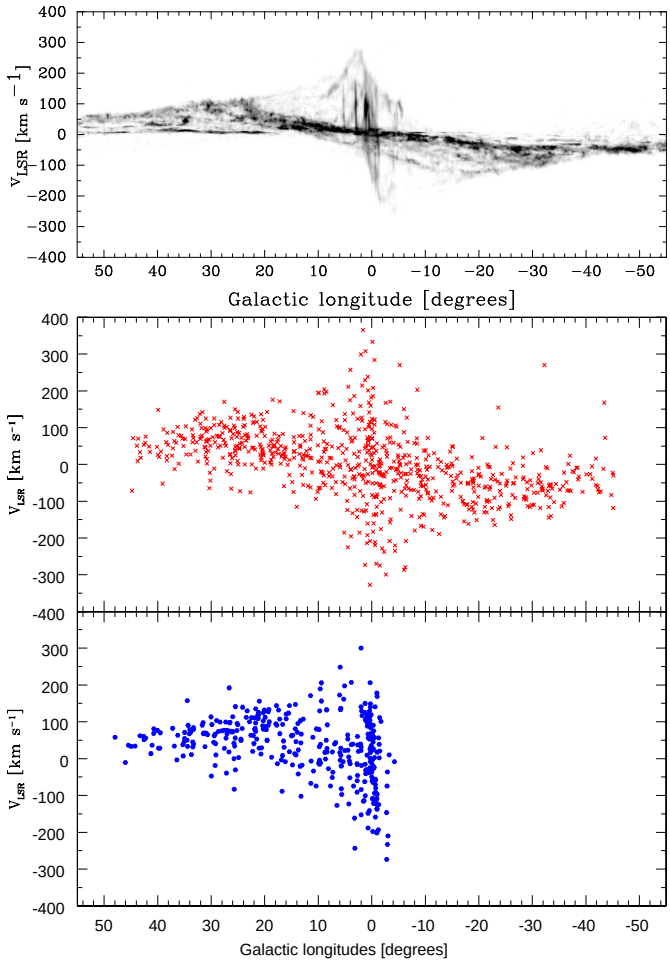

Figure 6.2: *Longitude–velocity diagrams. In the upper panel the CO distribution from Dame et al. (2001) is shown; the middle panel shows the sample of 766 OH/IR stars by Sevenster et al. (1997a,b, 2001); the lower panel shows the distribution of the 271 SiO masing stars from Chapter II plus another* ~ 90 *unpublished SiO maser detections.*

relation exists between terminal velocity and longitude: $v_{\rm term} = v_{\rm los}(R_{\rm tang}) - V_\odot \sin(l)$. This is plotted in Fig. 6.3, as two continuous curves, adopting a constant tangential velocity, $V_\odot$ of 220 km s^{-1}, all the way to the GC. The terminal velocity relation gives a good approximation to the highest velocity of the CO gas outside longitudes of about $\pm 20^\circ$, confirming that the gas in the Galactic plane moves largely in circular orbits around the GC. Most of the stars appear also constrained

by the same curve. However, since stars have higher velocity dispersions than the gas, some stars cross the edge defined by the gas terminal velocity by up to 60 km s^{-1}.

There is a lower density gas region at positive velocities between longitudes 20° and almost 0° and similarly at negative velocities and longitudes between 0° and −20°. Gas simulations show that a barred potential explains the gas distribution well, including the low–density regions (Athanassoula & Bureau 1999). Gas on intersecting orbits will collide with itself and a steady flow is not possible. The gas looses angular momentum and it will flow into smaller orbits at lower energies. Holes seem to appear also in the stellar $(l - v)$ diagram of the maser stars, but they can not be explained in the same way.

In the region close to the GC, not only the holes in the gas $(l - v)$ distribution, but also the presence of stars at forbidden velocities in the two quadrants ($l > 0$ and $v_{\rm los} < 0$) and ($l < 0$ and $v_{\rm los} > 0$) show that the assumption of circular orbits breaks down. In figure 6.3, where maser stars are over–plotted on the CO gas, the curve $-V_{\odot} \sin(l)$ is drawn. At positive (negative) longitudes the stars above (below) this curve could move on circular *prograde* orbits. This apparently applies to all maser stars in the longitude range $345^{\circ} > l > 15^{\circ}$. However, forbidden velocities at longitudes $|l| < 15^{\circ}$ are a clear sign of non–circular orbits. Both the OH and the SiO masers populate these regions within pretty much the same boundaries.

6.2.3 Nuclear Disk

The distribution of gas in the inner one degree from the Galactic centre, the circumnuclear zone (CMZ) or nuclear ring, is well described by a disk with a radius of about 200 pc radius (Combes 1991; Morris & Serabyn 1996). This disc appears in the $(l-v)$ diagram as a distinct feature: a strong correlation between longitude and velocity, at longitudes $-1.4 < l < 1.5^{\circ}$, with maximum velocities of about 200 km s^{-1}. Since the gas is a collisional medium, intersecting orbits are forbidden to gas. Dynamical models in a barred potential predict 2 kinds of orbits: X1, along the major axis of the bar, and X2 perpendicular to the X1. When the X1 start to be self–intersecting the gas moves inward in to the lower energy X2 orbits. The transition between the cusped X1 orbit and the X2 appear as a shock region where atomic gas is possibly converted in molecular gas. In principle, stars can populate the intersecting X1 orbits not accessible to gas clouds.

A strong correlation between longitude and velocity is seen also in the maser stars. It was first seen in OH/IR stars within 1° from the GC (Lindqvist et al. 1992; Sjouwerman et al. 1998) and clearly appears in our SiO maser stars (Fig. 6.2). A linear regression fit using the OH/IR stars gives a slope of 180 km s^{-1} pc^{-1} (Lindqvist et al. 1992), consistent with that derived for SiO targets (Chapter V).

As seen in Chapter V, nuclear disk stars are highly obscured ($A_{\rm K_S} > 2$ mag). The use of extinction estimates enabled us to exclude possible foreground objects and to select individual stellar members of the nuclear disk. Furthermore, since SiO targets are very bright at near–infrared wavelengths (Chapter III), they are

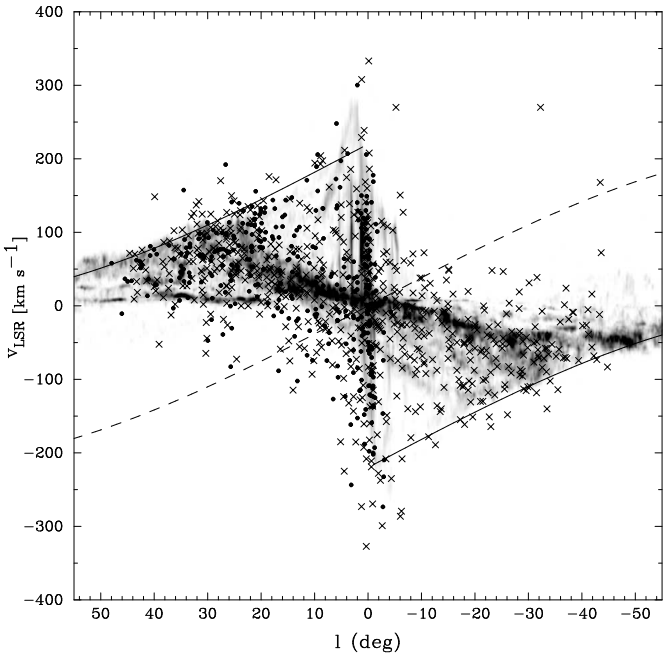

Figure 6.3: *This $(l-v)$ diagram shows the maser stars on the CO map. Symbols are as in Fig. 6.2. Continuous lines show the expected terminal velocities under the assumption of circular orbits. The dashed line is the curve $-V_\odot \sin(l)$, which corresponds to the opposite of the velocity of the Sun along the line-of-sight. At positive (negative) longitudes the stars on circular orbits above (below) this curve are moving prograde in the Galactic standard of rest. The remaining regions are then the forbidden regions.*

ideal for follow–up spectroscopic studies of the nuclear–disk population.

6.3 A simple dynamical model

In an axisymmetric potential, the angular momentum of each star, $L = r^2\,\partial\phi/\partial t$ is conserved and thus the stars will keep the same direction (i.e. $\partial\phi/\partial t$ will not change sign) when a star moves along its orbit. Clockwise moving stars (i.e. with positive line-of-sight velocity) seen at a positive longitude will move away from us (after correction for LSR motion). At negative longitudes these clockwise rotating stars are all coming toward us (i.e. $v_{\rm los}< 0$). In the $(l-v)$–diagram counter rotating stars will appear *only* in the "forbidden quadrants" ($l > 0$ and $v_{\rm los}< 0$) and ($l < 0$ and $v_{\rm los}> 0$).

Kinematic deviations from what would be expected in an axisymmetric poten-

tial were found by Sevenster et al. (2000), when modelling the underlying distribution function (DF). The observed line-of-sight dispersions for instance could not be explained by an axisymmetric model with σ_R equal to σ_z. Moreover, to explain the stars in the forbidden quadrants, isotropic components had to be invoked.

A barred potential explains the Galactic kinematics well. Several N–body dynamical models of the barred Milky Way exist (e.g. Fux 1997). They can be compared with observations qualitatively, but do not allow a real fit to the data. The latter is possible with the few dynamical models that are built by superposition of either (analytical) DF components (Sevenster et al. 2000) or of numerically integrated orbits (e.g. Häfner et al. 2000; Zhao 1996). The latter method is also known as Schwarzschild's method and is more general than the DF method, as it does not require a priori assumptions about the form of the DF, which is even more complicated by the fact that E_J is the only known integral of motion.

For the population of maser stars, no realistic dynamical model with a barred potential has yet been constructed. Therefore we started to calculate orbits in a barred potential with the ultimate goal to predict the observed distribution of maser points in the $(l - v)$ diagram. This is work under way, but the first results are promising. In the following we briefly sketch the various assumptions and steps made for our calculation and some first results.

6.3.1 Geometry

We adopt a Cartesian coordinate system (x, y, z), corotating with the bar–like bulge at a (clockwise) angular speed of $\Omega_b = 60$ km s^{-1} kpc^{-1}(Debattista et al. 2002). The origin of the coordinate system is at the Galactic centre, the x–axis is aligned with the major axis of the bar–like bulge and the y–axis with its minor axis. The Sun is assumed to lie at a distance $R_\odot$ from the Galactic centre, in the Galactic plane. The Sun-GC line makes an angle ϕ w.r.t. the long–axis of the bulge. We fix the Sun's distance to the Galactic centre at $R_\odot = 8$ kpc and its (clockwise) azimuthal velocity to $V_\odot = 200$ km s^{-1}. For a given mass model, this leaves two free parameters: the angular speed Ω_b of the bar-like bulge and the angle ϕ of the Sun w.r.t. to long–axis of this bulge.

6.3.2 Equations of motion

We calculate numerically the orbits of stars in a frame of reference that is rotating in the Galactic plane at an angular speed, $\vec{\Omega_b} = (0, 0, \Omega_b)$, solving the equation:

$$\ddot{\mathbf{r}} = -\nabla\Phi_{\text{eff}} - 2\left(\mathbf{\Omega_b} \times \dot{\mathbf{r}}\right). \tag{6.1}$$

In the right–hand side of this equation the first term is the acceleration induced by the effective gravitational potential; the second term is the Coriolis acceleration. The Coriolis acceleration introduces a dependence of the acceleration in the

x–direction on the velocity in the y–direction and vice versa. For further explanations see Binney & Tremaine (1987).

6.3.3 Gravitational potential

As a first qualitative study of the stellar dynamics in our Milky Way we consider the non–axisymmetric planar logarithmic potential (Binney & Tremaine 1987)

$$\Phi(x,y) = \frac{1}{2}v_0^2 \ln\left(R_C^2 + x^2 + \frac{y^2}{q^2}\right), \tag{6.2}$$

with constant velocity v_0, core radius R_C and axial ratio $q \leq 1$. Near the centre ($R \equiv \sqrt{x^2+y^2} \ll R_C$) the logarithmic potential approximates that of a two-dimensional harmonic oscillator, such that the corresponding central density is nearly homogeneous. Going outwards the rotation curve rapidly flattens to $v_c \sim v_0$. The constant axial ratio implies that the influence of the non–axisymmetry is similar at all radii. Although at larger radii this is not realistic for our Galaxy, the orbits calculated in this rotating potential are still representative as they become nearly circular beyond the corotation radius.

6.3.4 First results

Taking the above logarithmic potential with $v_0 = 200$ km s^{-1}, $R_C = 0.14$ kpc and $q = 0.9$, we calculated a set of closed orbits by numerically solving Eq. (6.1) with $\Omega_b = 60$ km s^{-1} kpc^{-1}. We used a fifth order Runge-Kutta algorithm as described in "Numerical Recipes" (Press et al. 1992). A representative example of these orbits in the XY-plane and in the $(l-v)$ diagram, is shown in Fig. 6.4.

We have just started these simulations and we need to further compare our model to observations in a quantitative way. However, as already proposed by Binney et al. (1991) for the gas, it clearly appears from the simple superposition of the orbits in the $(l-v)$ diagram that orbits from the X1 and X2 families can explain the observed forbidden stellar velocities.

6.4 Summary and future plans

In summary, the SiO and OH maser stars have a similar distribution in the velocity-longitude diagram. Their forbidden velocities are difficult to understand in an axisymmetric potential, but they can be understood in a rotating barred potential.

The disk maser stars beyond longitudes $|l| > 15^\circ$ are probably moving on loop orbits. Outside of the bar region the potential must be close to axisymmetry as observed in the terminal velocities of the gas.

For stars within longitudes $|l| < 15^\circ$, their forbidden velocities can be explained by X1/X2 orbits.

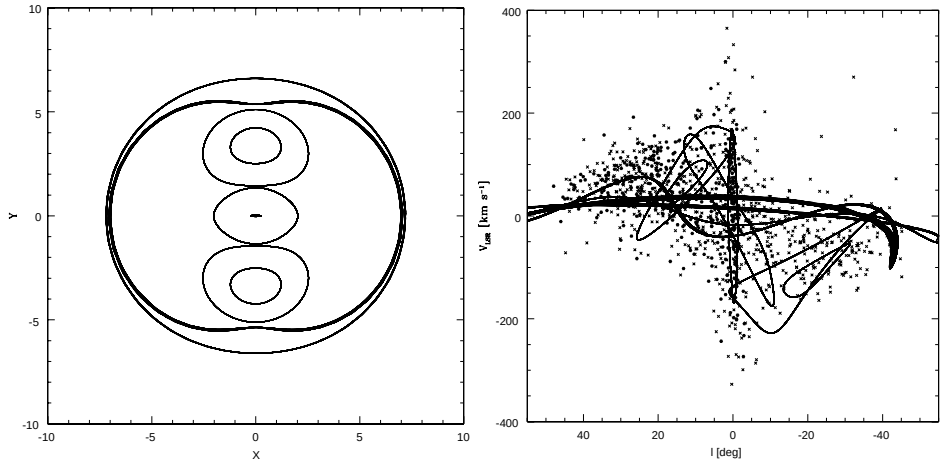

Figure 6.4: *Left panel: (x, y) plot of an example of closed orbits calculated in a rotating logarithmic potential (see text). Right panel: the same orbits projected in a $(l - v)$ diagram assuming $\phi = 45°$.*

The most realistic potential currently available is that obtained by the Basel group (Bissantz et al. 2003; Englmaier & Gerhard 1999). This is based on a mass model of the Milky Way derived from the dust corrected COBE maps. We plan to use the Basel potential to calculate a library of orbits and to fit these orbits to the available kinematics of maser stars. The fit can be done by maximising the likelihood of the line-of-sight velocity distribution at the (discrete) observations.

Acknowledgements. HH is grateful to the A&A Office in Paris for its kind support. Dr. Englmaier and Dr. Gerhard kindly provided us with their model of the Galactic potential.

References

Athanassoula, E. & Bureau, M. 1999, ApJ, 522, 699

Binney, J., Gerhard, O., & Spergel, D. 1997, MNRAS, 288, 365

Binney, J., Gerhard, O. E., Stark, A. A., Bally, J., & Uchida, K. I. 1991, MNRAS, 252, 210

Binney, J. & Tremaine, S. 1987, Galactic dynamics (Princeton, NJ, Princeton University Press, 1987, 747 p.)

Bissantz, N., Englmaier, P., & Gerhard, O. 2003, MNRAS, 340, 949

Blitz, L. & Spergel, D. N. 1991, ApJ, 379, 631

Combes, F. 1991, ARA&A, 29, 195

Dame, T. M., Hartmann, D., & Thaddeus, P. 2001, ApJ, 547, 792

de Vaucouleurs, G. 1964, in IAU Symp. 20: The Galaxy and the Magellanic Clouds, 195–+

Debattista, V. P., Gerhard, O., & Sevenster, M. N. 2002, MNRAS, 334, 355

Englmaier, P. & Gerhard, O. 1999, MNRAS, 304, 512

Fux, R. 1997, A&A, 327, 983

Häfner, R., Evans, N. W., Dehnen, W., & Binney, J. 2000, MNRAS, 314, 433

Lindqvist, M., Habing, H. J., & Winnberg, A. 1992, A&A, 259, 118

Messineo, M., Habing, H. J., Menten, K. M., Omont, A., & Sjouwerman, L. O. 2004a, A&A in preparation (Chapter V)

Messineo, M., Habing, H. J., Menten, K. M., Omont, A., & Sjouwerman, L. O. 2004b, A&A, 418, 103, Chapter III

Messineo, M., Habing, H. J., Sjouwerman, L. O., Omont, A., & Menten, K. M. 2002, A&A, 393, 115, Chapter II

Morris, M. & Serabyn, E. 1996, ARA&A, 34, 645

Nakada, Y., Onaka, T., Yamamura, I., et al. 1991, Nature, 353, 140

Paczynski, B., Stanek, K. Z., Udalski, A., et al. 1994, ApJ, 435, L113

Press, W. H., Teukolsky, S. A., Vetterling, W. T., & Flannery, B. P. 1992, Numerical recipes in FORTRAN. The art of scientific computing (Cambridge: University Press, —c1992, 2nd ed.)

Sevenster, M., Saha, P., Valls-Gabaud, D., & Fux, R. 1999, MNRAS, 307, 584

Sevenster, M. N. 1999a, MNRAS, 310, 629

Sevenster, M. N. 1999b, MNRAS, 310, 629

Sevenster, M. N. 2002, AJ, 123, 2772

Sevenster, M. N., Chapman, J. M., Habing, H. J., Killeen, N. E. B., & Lindqvist, M. 1997a, A&AS, 122, 79

Sevenster, M. N., Chapman, J. M., Habing, H. J., Killeen, N. E. B., & Lindqvist, M. 1997b, A&AS, 124, 509

Sevenster, M. N., Dejonghe, H., Van Caelenberg, K., & Habing, H. J. 2000, A&A, 355, 537

Sevenster, M. N., van Langevelde, H. J., Moody, R. A., et al. 2001, A&A, 366, 481

Sjouwerman, L. O., van Langevelde, H. J., Winnberg, A., & Habing, H. J. 1998, A&AS, 128, 35

Weiland, J. L., Arendt, R. G., Berriman, G. B., et al. 1994, ApJ, 425, L81

Whitelock, P. & Catchpole, R. 1992, in ASSL Vol. 180: The center, bulge, and disk of the Milky Way, 103

Zhao, H. S. 1996, MNRAS, 283, 149